Efficient kinetic method for fluid simulation beyond the Navier-Stokes equation

Raoyang Zhang,* Xiaowen Shan,† and Hudong Chen‡
Exa Corporation, 3 Burlington Woods Drive, Burlington, Massachusetts 01803, USA
(Received 26 January 2006; revised manuscript received 14 August 2006; published 12 October 2006)

We present a further theoretical extension to the kinetic-theory-based formulation of the lattice Boltzmann method of Shan *et al.* [J. Fluid Mech. **550**, 413 (2006)]. In addition to the higher-order projection of the equilibrium distribution function and a sufficiently accurate Gauss-Hermite quadrature in the original formulation, a regularization procedure is introduced in this paper. This procedure ensures a consistent order of accuracy control over the nonequilibrium contributions in the Galerkin sense. Using this formulation, we construct a specific lattice Boltzmann model that accurately incorporates up to third-order hydrodynamic moments. Numerical evidence demonstrates that the extended model overcomes some major defects existing in conventionally known lattice Boltzmann models, so that fluid flows at finite Knudsen number Kn can be more quantitatively simulated. Results from force-driven Poiseuille flow simulations predict the Knudsen's minimum and the asymptotic behavior of flow flux at large Kn.

DOI: 10.1103/PhysRevE.74.046703 PACS number(s): 47.11.−j, 47.45.Gx, 47.85.Np, 51.10.+y

I. INTRODUCTION

Understanding and simulating fluid flows possessing substantial nonequilibrium effects pose a long-standing challenge to fundamental statistical physics as well as to many other science and engineering disciplines [1,2]. Due to either rarefaction effects or small geometric scales, such flows are characterized by a finite Knudsen number, defined as the ratio between the particle mean free path l and the characteristic length L, $\mathrm{Kn}=l/L$. At sufficiently large Knudsen numbers, many of the continuum assumptions break down [3]. In particular, the Navier-Stokes equation and the no-slip boundary condition become inadequate.

Since the Boltzmann equation is valid for describing fluid flows at any Kn [4], the conventional approach for constructing extended hydrodynamic equations for higher-Kn regimes has been through employing higher-order Chapman-Enskog approximations resulting in, e.g, the Burnett and super-Burnett equations. However, this approach encounters both theoretical and practical difficulties [5,6]. Alternatively, attempts have been made to extend Grad's 13-moment system [7] by including contributions of higher kinetic moments [8]. One major difficulty has been the determination of the boundary condition for these moments because only the lowest few have clear physical meanings. In addition, due to the complexity in the resulting equations, application of this approach has been so far limited to simple one-dimensional situations. Nevertheless, the moment-based formulation offers an valuable insight into the basic fluid physics for high-Kn flows.

Over the past two decades, the lattice Boltzmann method (LBM) was developed into an efficient computational fluid dynamic (CFD) tool [9]. Due to its kinetic nature, the LBM intrinsically possesses some essential microscopic physics ingredients and is well suited for handling more general boundary conditions. Certain characteristic phenomena in microchannel flows were predicted in LBM simulations at least qualitatively [10–18]. In addition, by introducing a "stochastic virtual wall collision" process mimicking effects of free particle streaming in a long straight channel [14], analytically known asymptotic behavior at very large Kn was also produced. Nevertheless, being historically developed only to recover fluid physics at the Navier-Stokes level, the existing LBM schemes used in these studies possess some well-known inaccuracies and numerical artifacts. Therefore, strictly speaking the schemes are not applicable to high-Kn flows other than for some rather limited situations. It is important to develop an LBM method capable of performing accurate and quantitative simulations of high-Kn flows in general.

Recently, based on the moment expansion formulation [19], a systematic theoretical procedure for extending the LBM beyond the Navier-Stokes hydrodynamics was developed [20]. In this work, we present a specific extended LBM model from this procedure containing the next-order kinetic moments beyond the Navier-Stokes. A three-dimensional (3D) realization of this LBM model employs a 39-point Gauss-Hermite quadrature with a sixth-order isotropy. In addition, a previously reported regularization procedure [21,27], which is fully consistent with the moment expansion formulation, is incorporated and extended to the corresponding order. Simulations performed with the extended LBM have shown to capture certain characteristic features pertaining to finite-Kn flows. There is no empirical models used in our LBM.

II. BASIC THEORETICAL DESCRIPTION

It is theoretically convenient to describe a lattice Boltzmann equation according to the Hermite expansion representation [20]. The single-particle distribution functions at a set of particular discrete velocity values, $\{\boldsymbol{\xi}_a : a=1,\ldots,d\}$, are used as the state variables to describe a fluid system. The velocity-space discretization is shown to be equivalent to projecting the distribution function onto a subspace spanned

*Electronic address: raoyang@exa.com
†Electronic address: xiaowen@exa.com
‡Electronic address: hudong@exa.com

by the leading N Hermite orthonormal basis, denoted by $\mathbb{H}^N$ hereafter, provided that $\{\boldsymbol{\xi}_a\}$ are the abscissas of a sufficiently accurate Gauss-Hermite quadrature [19,20]. Adopting the Bhatnagar-Gross-Knook (BGK) collision model [22], the discrete distribution values f_a satisfy the following equation:

$$\frac{\partial f_a}{\partial t} + \boldsymbol{\xi}_a \cdot \nabla f_a = \Omega_a, \tag{1a}$$

$$\Omega_a = -\frac{1}{\tau}[f_a - f_a^{(0)}] + F_a, \quad a = 1, \ldots, d, \tag{1b}$$

where τ is a relaxation time, $f_a^{(0)}$ is the truncated Hermite expansion of the Maxwell-Boltzmann distribution evaluated at $\boldsymbol{\xi}_a$, and F_a is the contribution of the body force term. The truncation level determines the closeness of the above equation to approximate the original continuum BGK equation. A Chapman-Enskog analysis reveals that the Navier-Stokes equation is recovered when the second-order moment terms are retained. As the higher-order terms are included, physical effects beyond the Navier-Stokes can be captured systematically [20].

In this work we use a specific model of Eq. (1) that consists of moments up to the third order, one order higher than the Navier-Stokes hydrodynamics in conventional LBM models [9]. For our present investigation of flows at high Kn but low Mach numbers (Ma), here we set the temperature T to a constant for simplicity. Denoting the local fluid density and velocity by ρ and $\boldsymbol{u}$ and defining $u_a = \boldsymbol{\xi}_a \cdot \boldsymbol{u}$ for brevity, in the dimensionless units in which all velocities are normalized by the sound speed (i.e., $\sqrt{T}=1$), $f_a^{(0)}$ takes the following compact form:

$$f_a^{(0)} = w_a \rho \left[1 + u_a + \frac{u_a^2 - u^2}{2} + \frac{u_a(u_a^2 - 3u^2)}{6} \right], \tag{2}$$

where $u^2 = \boldsymbol{u} \cdot \boldsymbol{u}$ and w_a is the quadrature weight corresponding to the abscissa $\boldsymbol{\xi}_a$. The last term inside the brackets represents the contribution from the third-order kinetic moments [23] which was shown to be related to the velocity-dependent viscosity [24] but generally neglected in the conventional lattice Boltzmann models.

According to the previous analysis [20], the Gauss-Hermite quadrature employed for solving a third-order truncated system must be accurate with the polynomials up to the sixth order. For ease in implementing LBM model on Cartesian coordinates, we use the 3D Cartesian quadrature $E_{3,7}^{39}$ of Ref. [20]. Its 2D projection gives a quadrature $E_{2,7}^{21}$. The abscissas and weights of both quadratures are provided in Table I. Both LBM models can be verified to admit isotropy for tensors of the form $\Sigma w_a \boldsymbol{\xi}_a \cdots \boldsymbol{\xi}_a$ up to the sixth order instead of fourth in conventional LBM models. Explicitly speaking, recovery of the correct hydrodynamic physics up to the third order requires up to sixth-order isotropy conditions as follows [23]:

$$\sum_{a=1}^{d} w_a = 1, \tag{3a}$$

TABLE I. Degree-7 Gauss-Hermite quadratures on Cartesian grid. Listed are the number of points in the symmetry group p, abscissas ξ_a, and the weights w_a. Quadratures are named by the convention $E_{D,n}^d$ where the superscript d and subscripts D and n are, respectively, the number of abscissas, dimension, and degree of algebraic precision. The subscript FS denotes permutations with full symmetry. Note that since all velocities are normalized with sound speed, the Cartesian grid spacing has a unit velocity of $r=\sqrt{3/2}$.

Quadrature	p	ξ_a	w_a
$E_{3,7}^{39}$	1	(0, 0, 0)	1/12
	6	$(r,0,0)_{FS}$	1/12
	8	$(\pm r, \pm r, \pm r)$	1/27
	6	$(2r,0,0)_{FS}$	2/135
	12	$(2r,2r,0)_{FS}$	1/432
	6	$(3r,0,0)_{FS}$	1/1620
$E_{2,7}^{21}$	1	(0, 0)	91/324
	4	$(r,0)_{FS}$	1/12
	4	$(\pm r, \pm r)$	2/27
	4	$(2r,0)_{FS}$	7/360
	4	$(\pm 2r, \pm 2r)$	1/432
	4	$(3r,0)_{FS}$	1/1620

$$\sum_{a=1}^{d} w_a \xi_{a,i} \xi_{a,j} = \delta_{ij}, \tag{3b}$$

$$\sum_{a=1}^{d} w_a \xi_{a,i} \xi_{a,j} \xi_{a,k} \xi_{a,l} = \delta_{ijkl}^{(4)}, \tag{3c}$$

$$\sum_{a=1}^{d} w_a \xi_{a,i} \xi_{a,j} \xi_{a,k} \xi_{a,l} \xi_{a,m} \xi_{a,n} = \delta_{ijklmn}^{(6)}, \tag{3d}$$

where the subscripts $i, j, \ldots, n$ denote Cartesian components. In the above, δ_{ij} is the Kronecker delta function, while $\delta_{ijkl}^{(4)}$ and $\delta_{ijklmn}^{(6)}$ represent, respectively, the fourth- and sixth-order generalizations:

$$\delta_{ijkl}^{(4)} = \delta_{ij}\delta_{kl} + \delta_{ik}\delta_{jl} + \delta_{il}\delta_{jk},$$

$$\delta_{ijklmn}^{(6)} = \delta_{ij}\delta_{klmn}^{(4)} + \delta_{ik}\delta_{jlmn}^{(4)} + \delta_{il}\delta_{jkmn}^{(4)} + \delta_{im}\delta_{jkln}^{(4)} + \delta_{\mathrm{in}}\delta_{jklm}^{(4)}. \tag{4}$$

Indeed, direct verification shows that these are satisfied by the 3D 39-speed model ($E_{3,7}^{39}$) and its 2D projection ($E_{2,7}^{21}$). The conventional LBM schemes only satisfy the above moment isotropy conditions up to the fourth order (i.e., the Navier-Stokes order). It is also important to mention that there exist a few other lattice Boltzmann models satisfying sixth-order isotropy [25,26]. However, they contain more discrete speeds and more complicated coefficients, and are difficult to extend to even higher orders.

With the Cartesian quadrature above, Eq. (1a) can be directly discretized in physical space and time, yielding a standard lattice Boltzmann equation of the form

$$f_a(\boldsymbol{x}+\boldsymbol{\xi}_a,t+1)=f_a(\boldsymbol{x},t)-\frac{1}{\tau}[f_a(\boldsymbol{x},t)-f_a^{(0)}]+F_a. \quad (5)$$

As usual, the "lattice convention" with unity time increment is used here.

III. REGULARIZATION PROCEDURE

An LBM computation is generally carried out in two steps: the streaming step in which f_a at $\boldsymbol{x}$ is moved to $\boldsymbol{x}+\boldsymbol{\xi}_a$ and the collision step in which $f_a(\boldsymbol{x})$ is replaced with the right-hand side of Eq. (5). When viewed as a projection of the continuum BGK equation into $\mathbb{H}^N$, this dynamic process introduces an error due to the fact that f_a does not automatically lie entirely within $\mathbb{H}^N$. Borrowing language from spectral analysis, this is analogous to the aliasing effect. When the system is not far from equilibrium, such an error is small and ignorable. On the other hand, this error can be resolved via an extension of the "regularization procedure" previously designed for improvement in stability and isotropy [21,27]. In terms of the Hermite expansion interpretation, the regularization procedure is more concisely described as the following. We split the post-streaming distribution into two parts:

$$f_a=f_a'+f_a^{(0)}, \quad (6)$$

where f_a' is the deviation from the truncated Maxwellian, or the *nonequilibrium* part of the distribution. As $f_a^{(0)}$ already lies entirely in the subspace $\mathbb{H}^N$, the projection is to ensure that the nonequilibrium contribution also lies in the same subspace for all times and only needs to be applied to f_a'. Effectively, the projection serves as a filtering (or "dealiasing") process to ensure the system stay inside the defined subspace $\mathbb{H}^N$ in a Galerkin interpretation.

The projection is to convert f_a' to a new distribution $\hat{f}_a'$ which lies within the subspace spanned by the first three Hermite polynomials. Using the orthogonality relation of the Hermite polynomials and the Gauss-Hermite quadrature, $\hat{f}_a'$, is given by the pair of relations

$$\hat{f}_a'=w_a\sum_{n=0}^{3}\frac{1}{n!}\boldsymbol{a}^{(n)}\mathcal{H}^{(n)}(\boldsymbol{\xi}_a), \quad a=1,\ldots,d, \quad (7a)$$

$$\boldsymbol{a}^{(n)}=\sum_{a=1}^{d}f_a'\mathcal{H}^{(n)}(\boldsymbol{\xi}_a), \quad n=0,\ldots,3, \quad (7b)$$

where $\mathcal{H}^{(n)}$ is the standard nth Hermite polynomial [19,28]:

$$\mathcal{H}^{(0)}(\boldsymbol{\xi})=1, \quad (8a)$$

$$\mathcal{H}_i^{(1)}(\boldsymbol{\xi})=\xi_i, \quad (8b)$$

$$\mathcal{H}_{ij}^{(2)}(\boldsymbol{\xi})=\xi_i\xi_j-\delta_{ij}, \quad (8c)$$

$$\mathcal{H}_{ijk}^{(3)}(\boldsymbol{\xi})=\xi_i\xi_j\xi_k-\xi_i\delta_{jk}-\xi_j\delta_{ik}-\xi_k\delta_{ij}, \quad (8d)$$

and $\boldsymbol{a}^{(n)}$ the corresponding Hermite expansion coefficient, both rank-n tensors. The first two Hermite coefficients vanish due to the vanishing contribution from the nonequilibrium distribution to mass and momentum. The second and third Hermite coefficients are

$$\boldsymbol{a}^{(2)}=\sum_{a=1}^{d}f_a'\boldsymbol{\xi}_a\boldsymbol{\xi}_a, \quad \boldsymbol{a}^{(3)}=\sum_{a=1}^{d}f_a'\boldsymbol{\xi}_a\boldsymbol{\xi}_a\boldsymbol{\xi}_a, \quad (9)$$

where $\boldsymbol{a}^{(2)}$ is traceless due to the conservation of energy. Clearly from the above construction or from direct verification, the projected distribution $\hat{f}_a'$ gives the same second-order (momentum) and third-order fluxes as the original f_a',

$$\sum_{a=1}^{d}\hat{f}_a'\boldsymbol{\xi}_a\boldsymbol{\xi}_a=\sum_{a=1}^{d}f_a'\boldsymbol{\xi}_a\boldsymbol{\xi}_a, \quad (10a)$$

$$\sum_{a=1}^{d}\hat{f}_a'\boldsymbol{\xi}_a\boldsymbol{\xi}_a\boldsymbol{\xi}_a=\sum_{a=1}^{d}f_a'\boldsymbol{\xi}_a\boldsymbol{\xi}_a\boldsymbol{\xi}_a. \quad (10b)$$

This is an essential step to preserve the required nonequilibrium properties affecting macroscopic physics. Furthermore, unlike f_a' in which all higher-order moments are in principle present, the projected distribution $\hat{f}_a'$ can be shown via the orthogonality argument to give zero contributions to fluxes higher than the defined third order above. Consequently, its physical implication is rather apparent: The regularization procedure filters out the higher-order nonequilibrium moments that contain strong discrete artifacts due to the insufficient support of the lattice basis.

Overall, given the discrete nonequilibrium distribution, its projection in $\mathbb{H}^3$ is fully specified by

$$\hat{f}_a'=w_a\left[\frac{\mathcal{H}^{(2)}(\boldsymbol{\xi}_a)}{2}\sum_{b=1}^{d}f_b'\boldsymbol{\xi}_b\boldsymbol{\xi}_b+\frac{\mathcal{H}^{(3)}(\boldsymbol{\xi}_a)}{6}\sum_{b=1}^{d}f_b'\boldsymbol{\xi}_b\boldsymbol{\xi}_b\boldsymbol{\xi}_b\right]. \quad (11)$$

Incorporating the regularization procedure, Eq. (5) is modified to become

$$f_a(\boldsymbol{x}+\boldsymbol{\xi}_a,t+1)=f_a^{(0)}+\left(1-\frac{1}{\tau}\right)\hat{f}_a'+F_a. \quad (12)$$

It is revealing to realize that the right-hand side represents a damping operator acting on the "nonequilibrium" part of the dsitribution function. It is an immediate extension to assign a different relaxation time to each individual Hermite mode. Namely, we can recast the collision operator into an equivalent yet slightly more general form

$$\Omega_a=\sum_{b=1}^{d}\mathcal{M}_{ab}f_b', \quad (13)$$

where the linear matrix operator takes the following generic form:

$$\mathcal{M}_{ab} \equiv \delta_{ab} + \left(1 - \frac{1}{\tau}\right) w_a \left[\theta_1 \frac{\mathcal{H}^{(2)}(\boldsymbol{\xi}_a)}{2} \boldsymbol{\xi}_b \boldsymbol{\xi}_b + \theta_2 \frac{\mathcal{H}^{(3)}(\boldsymbol{\xi}_a)}{6} \boldsymbol{\xi}_b \boldsymbol{\xi}_b \boldsymbol{\xi}_b \right]. \quad (14)$$

The additional coefficients θ_1 and θ_2 can have values between 0 and 1 separately. Indeed, when $\theta_1=\theta_2=1$, then we recover the result in Eq. (11), the third-order accurate projection operator. On the other hand, comparing Eq. (14) with the similar expression in Ref. [21], we find that the latter is in fact a second-order projection operator [i.e., the first term in Eq. (14)], or simply $\theta_1=1$ and $\theta_2=0$. It is to be emphasized that the correct application of the third-order projection operator is based on the necessary condition of the third-order Hermite quadrature. Hence it cannot be realized via conventional low-order LBM such as the popular D3Q19 (or D2Q9).

The explicit form of the body force term comes directly from the Hermite expansion of the continuum BGK equation [20,29]. Up to the third order, it can be expressed as

$$F_a = w_a \rho \boldsymbol{g} \cdot (\boldsymbol{\xi}_a + u_a \boldsymbol{\xi}_a - \boldsymbol{u}) + \frac{1}{2} w_a [\boldsymbol{a}^{(2)} + \rho \boldsymbol{u}\boldsymbol{u}] : [g_a \mathcal{H}^{(2)}(\boldsymbol{\xi}_a) - 2\boldsymbol{g}\boldsymbol{\xi}_a]. \quad (15)$$

To be noted here is that, whereas the first terms is entirely due to the equilibrium part of the distribution, the terms related to $\boldsymbol{a}^{(2)}$ are contributions from the nonequilibrium part. To our knowledge, the nonequilibrium contribution in the body force has not been explicitly considered in the existing LBM literature. Nevertheless, although it is expected to play an important role at large Kn, at moderate Kn ($\leqslant 1$), no significant effects due to the nonequilibrium contribution are observed in the numerical experiments in the present work.

IV. NUMERICAL RESULTS

A. Shear wave decay

The first series of numerical simulations performed are for the benchmark problem of 2D sinusoidal shear wave decay. This set of tests is to evaluate impact from the increased order of accuracy and from the regularization procedure on the resulting isotropy. Obviously, a numerical artifact-free wave decay should not depend on its relative orientation with respect to the underlying lattice orientation. The lattice-orientation-dependent artifact has often plagued discrete fluid models especially at finite Knudsen number when nonequilibrium effects are significant. For this purpose, we have defined two sets of simulations. In the first set, a sinusoidal wave with a wavelength (L) of 128 grid spacing is simulated on a 128×128 periodic domain. The initial velocity field is given by $u_x = u_0 \sin(y/2\pi L)$ and $u_y=0$. The wave vector is aligned with the lattice. In the second set, the same sinusoidal wave is rotated by 45° from the original orientation and simulated on a matching periodic domain size of 181 $(=128\sqrt{2}) \times 181$. The Knudsen number, defined as $\mathrm{Kn}=2\tau c_s/L$, is chosen to be 0.2, where τ is the relaxation time and c_s the sound speed. These two sets of simulations were conducted using four representative models: the popular 2D 9-state (9-s) model (D2Q9) and the present 2D 21-state (21-s) model based on $E^{21}_{2,7}$, both with and without the regularization process. Note that the 2D 9-state model only admits a second-order regularization projection as discussed in the preceding section. In discussions hereafter we shall refer the models without the regularization as the BGK models and the ones with regularization the REG models.

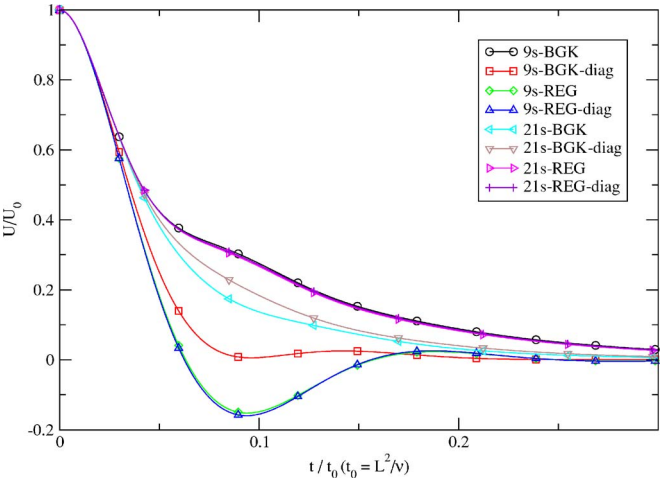

FIG. 1. (Color online) Peak velocity of a decaying shear waves as simulated by the 9-state (9-s) and the 21-state (21-s) standard BGK and regularized (REG) models. For each model, simulation is carried out with the wave vector aligned with either the lattice links or their diagonals. The latter is denoted by the post-fix "diag."

In Fig. 1, the dimensionless peak velocity magnitude, normalized by its initial value and measured at the 1/4 width of wavelength, is plotted against the nondimensionalized time normalized by the characteristic decay time $t_0=L^2/\nu$, where $\nu=c_s^2(\tau-1/2)$ is the kinematic viscosity. As one can easily notice, the decay rate of the shear wave for the 9-s BGK model is substantially different between the lattice oriented setup and the 45° one, exhibiting a strong dependence on the orientation of the wave vector with respect to the lattice. This indicates a strong anisotropy of the model at this Kn. This is consistent with our expectation that the 9-s BGK model was originally formulated to only recover the Navier-Stokes hydrodynamics (i.e., at vanishing Kn). Interestingly this anisotropy is essentially eliminated by the second-order regularization procedure in the resulting 9-s REG model. On the other hand, the amplitude of the shear wave exhibits a strong oscillatory behavior in addition to the exponential decay, implying a greater than physical ballistic effect. These may be explained as the following: The nonequilibrium part of the post-streaming distribution contains contributions from *in principle* all moments, which are highly anisotropic due to inadequate (only up to the second-order moment) symmetry in the underlying discrete model. The regularization procedure filters out all the higher than second-order moment contributions, yielding an isotropic behavior supported by the given lattice. On the other hand, the higher moments are critical at large Kn. Therefore, though isotropic, the 9-s REG model still should not be expected to show satisfactory physical results at high Knudsen numbers. For the 21-s BGK

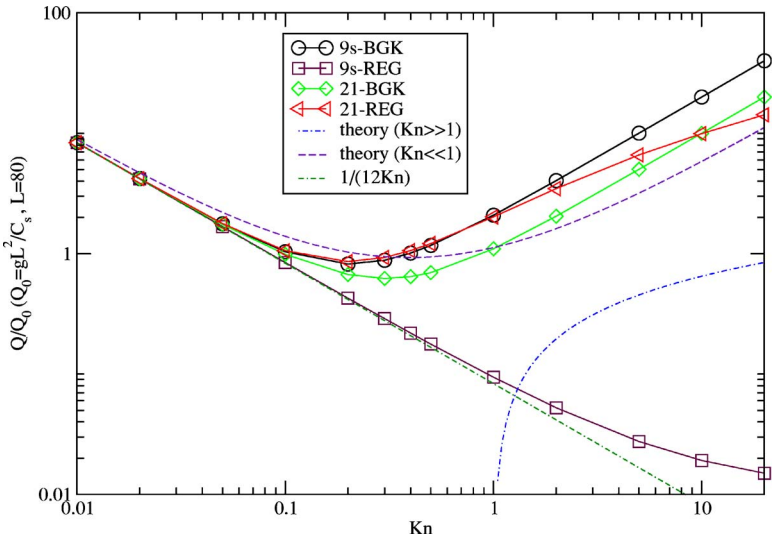

FIG. 2. (Color online) Knudsen paradox with resolution 40, $\mathrm{Ma}=1.46\times10^{-6}$. The Kn which has the minimum Q is about 0.2 for 21-s REG, 0.3 for 21-s BGK and 0.2 for 9-s BGK models. The theoretical results are those of Cercignani [4].

model, an anisotropic behavior is also very visible, though to a much smaller extent. This may be attributed to the residual anisotropy in moments higher than the third order. Again, the anisotropy behavior is completely removed once the regularization procedure is applied in the 21-s REG model, as shown from the totally overlapped curves between the lattice-oriented and diagonal-oriented simulations. It is also noticeable that the decay history shows a much reduced oscillatory behavior in the 21-s REG model. Because of its correct realization of the third-order moment flux, we expect that the result is more accurate at this Knudsen number value. It is also curious to observe that the decay of the "lattice-aligned" result from 9-s BGK is surprisingly close to that of the 21-s REG model at this Kn. This is likely to be a mere coincidence.

B. Finite-Knudsen-number channel flows

Using the same four models, we subsequently carried out simulations of the force-driven Poiseuille flow for a range of Knudsen numbers. In order to identify the impact in accuracy in the resulting lattice Boltzmann models as opposed to the effects from various boundary conditions, here a standard halfway bounce-back boundary condition is used in the cross-channel (y) direction. Furthermore, since we are not interested, for the present study, in any physical phenomenon associated with streamwise variations, a periodic boundary condition is used with only four grid points in the streamwise (x) direction. In the cross-stream (y) direction, two different resolutions $L=40$ and 80 are both tried to ensure sufficient resolution independence. The Knudsen number is defined as $\mathrm{Kn}=\nu/(c_sL)$. The flow is driven by a constant gravity force $\boldsymbol{g}$ pointing in the positive-x direction. The magnitude of the force is set to $8\nu U_0/L^2$, which would give rise to a parabolic velocity profile with a peak velocity of U_0 in the vanishing Kn limit. For consistence, a modified definition of fluid velocity, $\boldsymbol{u}\rightarrow\boldsymbol{u}+\boldsymbol{g}/2$, is used in $f_a^{(0)}$. Since the LBM models presently used here all assume a constant temperature, to enforce an incompressible behavior with negligible thermodynamic effect throughout the simulated Kn range, we choose a sufficiently small value of U_0, corresponding to the nominal Mach numbers of Ma $(=U_0/c_s)\sim1.46\times10^{-6}$ and 2.92×10^{-7}, and verified that our results are independent of Ma. The actual resulting fluid velocity in these simulations can achieve values much higher than U_0 at higher Kn.

Plotted in Fig. 2 is the nondimensionalized mass flux $Q\equiv\Sigma_{y=0}^{L}u_x(y)/Q_0$ as a function of Kn in the final steady state of the simulations. Here $Q_0=gL^2/c_s$. For comparison we also include two analytical asymptotic solutions [4] for both small and very large Kn. To be noted first is that at the vanishing Kn limit, all simulation results agree with each other as well as with the analytical solution. This confirms that all these LBM schemes recover the correct hydrodynamic behavior at vanishing Kn—i.e., the Navier-Stokes limit. Also plotted is the exact Navier-Stokes solution of $Q=1/(12\mathrm{Kn})$, a well-understood monotonically decreasing line with no minimum. At higher Kn, the 9-s BGK model exhibits a Knudsen's minimum while it overestimates the flux according to some previously published reports [14]. However, by filtering out moment contributions higher than the second order, such a phenomenon is completely disappeared from the result of 9-s REG, yielding a purely monotonically decreasing behavior. This is a rather interesting but not entirely surprising result. Once again, the regularization process enforces the system to be confined within the second-order Hermite moment space, while all higher-order nonequilibrium contributions including both the numerical artifacts and the physical ones, responsible for the finite Knudsen phenomena, are filtered out. Consequently, only the Navier-Stokes order effects are preserved in the 9-s REG model no matter the degree of nonequilibrium at finite Kn. To be further noticed is the impact of the second-order regularization on the near-wall properties. In particular, Fig. 3 shows that 9-s REG gives vanishing slip velocity at the wall for a range of Kn values (Kn=0.1, 0.2, and 0.5). This suggests that a bounce-back boundary process is sufficient to realize a no-slip condition once a Navier-Stokes order dynamics in the model equation is enforced. This is yet another confirmation as to why the resulting Q from the 9-s REG model lies very close to the exact Navier-Stokes theoretical curve up to significantly high Kn values. In comparison, all

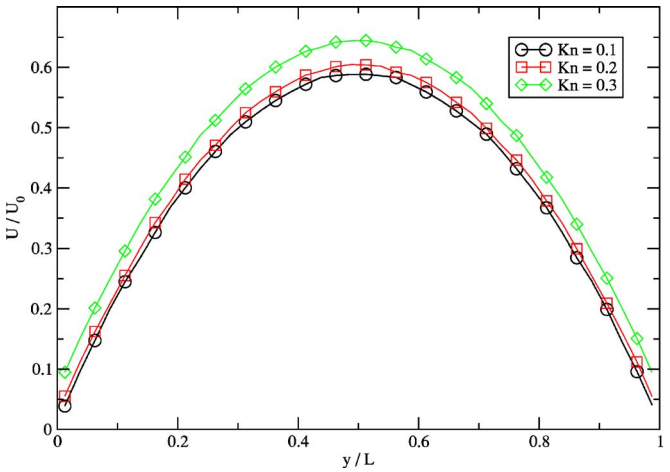

FIG. 3. (Color online) Normalized velocity profiles at resolution 40 and Kn=0.1, 0.2, and 0.5. Notice the 9-s REG model exhibits no visible slip velocity for both small and large Kn.

the other three LBM models show finite slip velocity values, due to the previous discussed reason that they all contain higher than second-order nonequilibrium contributions. Once again, one must remember that the higher order effects in the 9-s BGK model (and to a lesser extent the 21-s BGK model) have substantial lattice discrete artifacts. To be emphasized is the 21-s REG model: Due to the regularization procedure, only up to the third-order nonequilibrium moment contribution is preserved. On the other hand, because it has been numerically shown to capture the Knudsen minimum phenomenon, correct incorporation of the third-order moment physics is thus essential for accurately simulating some key flow physics beyond the Navier-Stokes. We also wish to emphasize that all these differences are due to the intrinsic nature of these LBM models and has nothing to do with spatial and temporal resolutions. As a comparison, we plot in Fig. 4 velocity profiles generated from the 21-s REG model.

There are a number of ways that gravity force can be included in LB equations. One can either treat the gravity force outside the collision operator as an external body force term as given by Eq. (15) or by applying a local momentum-velocity shift inside the equilibrium distribution [30]. With the regular BGK model, for all Kn, no difference in results are observed when the gravity force is applied in different ways. With the regularization procedure and sufficient isotropy, however, some differences are observed at finite (>1) Kn. Generally speaking, applying the body force via Eq. (15) tends to predict higher flux then via momentum-velocity shifting. For the results shown in Fig. 2, the velocity shift applied in $f_a^{(0)}$ is $1/2g$. The other half of the gravity force is applied as an external body force term (15) (cf. [29]).

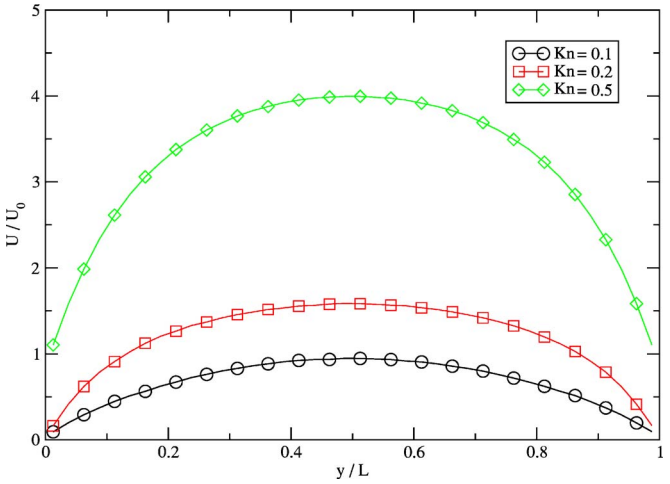

FIG. 4. (Color online) Normalized velocity profiles at resolution 40 and Kn=0.1, 0.2, and 0.5. Notice the 21-s REG model exhibits substantial slip velocity at large Kn.

The results from both the 21-s BGK and the 21-s REG models predict a Knudsen minimum which resembles that of the 9-s BGK except with reduced overestimations at higher Kn. What is interesting, and requires further understanding, is that the flux behavior predicted by the 21-s REG model exhibits a reversal of curvature at higher Kn, resembling the analytical asymptotic solution of Cercignani [4].

The qualitative differences seen from these four models suggest that contributions from moments beyond second order are essential for capturing fundamental physical effects at high Kn. Although the high-order moments are implicitly contained in the second-order BGK model, its dynamics is highly contaminated with numerical lattice artifacts. In contrast, by incorporating the high-order moments explicitly and systematically with the regularization, flows at these Kn values can indeed be captured by the extended LBM model.

V. CONCLUSION

In summary, the kinetic-based representation offers a well-posed approach in formulations of computational models for performing efficient and quantitative numerical simulations of fluid flows at finite Kn. In this work we present a specific extended LBM model that accurately incorporates the physical contributions of kinetic moments up to the third order in Hermite expansion space. The regularization procedure presented in this paper ensures that both the equilibrium and nonequilibrium effects are confined in the accurately supported truncated subspace at all times so that the unphysical artifacts are filtered out in the dynamic process. This resulting LBM model is robust and highly efficient. Because of its accurate inclusion of the essential third-order contributions, this model is demonstrated to be capable of quantitatively capturing certain fundamental flow physics properties at finite Knudsen numbers. This is accomplished without imposing any empirical models. Furthermore, because of the removal of discrete anisotropy, it is also clear that the LBM model is not limited to specific unidirectional channel flows; nor is it only applicable for lattice-aligned orientations.

Nevertheless, a number of issues await further studies. For even higher Kn (~ 10), one should expect moment contributions higher than the third order to become physically important. This is straightforward to include via the systematic formulation [20] together with the regularization procedure described here. The issue of boundary condition is also of crucial importance [31–33], even though, as demonstrated in this paper, the realization of the essential slip-velocity ef-

fect and the asymptotic behavior is attributed *to a significant extent* to the third-order and higher-moment contributions in the intrinsic LBM dynamic model itself. As reported in some previous works [13,14], the kinetic boundary condition of Ansumali and Karlin [34] has led to substantial improvements in Navier-Stokes-level microchannel flow simulations. The boundary condition itself serves as an effective collision so that it also modifies the degree of the nonequilibrium distribution. Specifically, the well-known Maxwell boundary condition (in which the particle distribution function is assumed to be at equilibrium) should be expected give different effect at high Kn compared with that of the bounce-back used in the present study. The latter boundary condition preserves nonequilibrium contributions at all orders. As a consequence, we suspect that the finite slip phenomenon is likely to still be over predicted in our current simulations with the bounce-back boundary condition than what actually would occur in reality. Many more detailed and further investigations particularly pertaining channel flows at finite Knudsen number are certainly extremely important in the future studies.

Thermodynamic effect is also expected to become important at finite Kn when the Mach number is not negligibly small, some distinctive phenomena that are substantial and characteristic only at finite Knudsen numbers with sufficiently large Mach numbers [35]. The work of Xu [35] demonstrates the importance of an accurate formulation of higher than the Navier-Stokes order thermodynamic effect at finite Kn. Theoretically, this additional property is associated with the so-called super-Burnett effect in more conventional language [35], or the fourth-order moment contribution in the Hermite expansion, and can be incorporated in a further extended LBM model [20]. The present third-order model is thermodynamically consistent, but only at the Navier-Stokes level [20]. Another interesting point to mention is that both the 21-s BGK or the 21-s REG models can allow an expanded equilibrium distribution form including terms up to the fourth power in fluid velocity (as opposed to the square power in 9-s BGK), such that the correct equilibrium energy flux tensor is still preserved. Including the fourth-power terms immediately results in a desirable positive-definite distribution for the zero-velocity state at all Mach number values.

ACKNOWLEDGMENT

The work was supported in part by the National Science Foundation.

[1] J. M. Reese, M. A. Gallis, and D. A. Lockerby, Philos. Trans. R. Soc. London, Ser. A **361**, 2967 (2003).
[2] C.-M. Ho and Y.-C. Tai, Annu. Rev. Fluid Mech. **30**, 579 (1998).
[3] M. Gad-el-Hak, J. Fluids Eng. **121**, 5 (1999).
[4] C. Cercignani, *Theory and Application of the Boltzmann Equation* (Scottish Academic Press, New York, 1974).
[5] R. K. Standish, Phys. Rev. E **60**, 5175 (1999).
[6] R. K. Agarwal, K.-Y. Yun, and R. Balakrishnan, Phys. Fluids **13**, 3061 (2001).
[7] H. Grad, Commun. Pure Appl. Math. **2**, 331 (1949).
[8] H. Struchtrup, Phys. Rev. E **65**, 041204 (2002).
[9] S. Chen and G. Doolen, Annu. Rev. Fluid Mech. **30**, 329 (1998).
[10] X. Nie, G. D. Doolen, and S. Chen, J. Stat. Phys. **107**, 279 (2002).
[11] C. Y. Lim, C. Shu, X. D. Niu, and Y. T. Chew, Phys. Fluids **14**, 2299 (2002).
[12] B. Li and D. Y. Kwok, Phys. Rev. Lett. **90**, 124502 (2003).
[13] X. D. Niu, C. Shu, and Y. T. Chew, Europhys. Lett. **67**, 600 (2004).
[14] F. Toschi and S. Succi, Europhys. Lett. **69**, 549 (2005).
[15] Y. Zhou, R. Zhang, I. Staroselsky, H. Chen, W. Kim, and M. S. Jhon, Physica A **362**, 68 (2006).
[16] S. Ansumali and I. V. Karlin, Phys. Rev. Lett. **95**, 260605 (2005).
[17] S. Ansumali, I. Karlin, C. E. Frouzakis, and K. Boulouchos, Physica A **359**, 289 (2006).
[18] Z. Guo, T. S. Zhao, and Y. Shi, J. Appl. Phys. **99**, 074903 (2006).
[19] X. Shan and X. He, Phys. Rev. Lett. **80**, 65 (1998).
[20] X. Shan, X.-F. Yuan, and H. Chen, J. Fluid Mech. **550**, 413 (2006).
[21] H. Chen, R. Zhang, I. Staroselsky, and M. Jhon, Physica A **362**, 125 (2006).
[22] P. L. Bhatnagar, E. P. Gross, and M. Krook, Phys. Rev. **94**, 511 (1954).
[23] H. Chen, C. Teixeira, and K. Molvig, Int. J. Mod. Phys. C **8**, 675 (1997).
[24] Y.-H. Qian and Y. Zhou, Europhys. Lett. **42**, 359 (1998).
[25] Y. Chen, H. Ohashi, and M. Akiyama, Phys. Rev. E **50**, 2776 (1994).
[26] M. Watari and M. Tsutahara, Phys. Rev. E **70**, 016703 (2004).
[27] J. Latt and B. Chopard, Math. Comput. Simul. **72**, 165 (2006).
[28] H. Grad, Commun. Pure Appl. Math. **2**, 325 (1949b).
[29] N. S. Martys, X. Shan, and H. Chen, Phys. Rev. E **58**, 6855 (1998).
[30] X. Shan and H. Chen, Phys. Rev. E **47**, 1815 (1993).
[31] I. Ginzburg and P. M. Adler, J. Phys. II **4**, 191 (1994).
[32] I. Ginzburg and D. d'Humières, J. Stat. Phys. **84**, 927 (1995).
[33] H. Chen, C. Teixeira, and K. Molvig, Int. J. Mod. Phys. C **9**, 1281 (1998).
[34] S. Ansumali and I. V. Karlin, Phys. Rev. E **66**, 026311 (2002).
[35] K. Xu, Phys. Fluids **15**, 2077 (2003).